Optical Vortex Brillouin Laser

Xinglin Zeng,* Philip St. J. Russell, Yang Chen, Zheqi Wang, Gordon K. L. Wong, Paul Roth, Michael H. Frosz, and Birgit Stiller

Optical vortices, which have been extensively studied over the last decades, offer an additional degree of freedom useful in many applications, such as optical tweezers and quantum control. Stimulated Brillouin scattering (SBS), providing a narrow linewidth and a strong nonlinear response, has been used to realize quasi-continuous wave lasers. Here, stable oscillation of optical vortices and acoustic modes in a Brillouin laser based on chiral photonic crystal fiber (PCF) is reported, which robustly supports helical Bloch modes (HBMs) that carry circularly polarized optical vortex and display circular birefringence. A narrow-linewidth Brillouin fiber laser that stably emits 1st- and 2nd-order vortex-carrying HBMs is implemented. Angular momentum conservation selection rules dictate that pump and backward Brillouin signals have opposite topological charge and spin. Additionally, it is shown that when the chiral PCF is placed within a laser ring cavity, the linewidth-narrowing associated with lasing permits the peak of the Brillouin gain that corresponds to acoustic mode to be measured with resolution of 10 kHz and accuracy of 520 kHz. The results pave the way to a new generation of vortex-carrying SBS systems with applications in optical tweezers, quantum information processing, and vortex-carrying nonreciprocal systems.

1. Introduction

Stimulated Brillouin scattering (SBS) in optical fibers, in which guided light is parametrically reflected by coherent acoustic phonons, provides a powerful and flexible mechanism for controlling light. Since its first demonstration,[1] SBS has been explored and exploited in many different systems, especially optical fibers[2] and integrated photonics.[3] Among the many applications of SBS, the Brillouin laser is one of the most exploited and important, offering great flexibility in many contexts, for example optical sensors,[4] microwave oscillators,[5] and optical gyroscopes.[6]

X. Zeng, P. S. J. Russell, Y. Chen, Z. Wang, G. K. L. Wong, P. Roth, M. H. Frosz, B. Stiller
Max-Planck Institute for the Science of Light
Staudtstr. 2, 91058 Erlangen, Germany
E-mail: xinglin.zeng@mpl.mpg.de
B. Stiller
Department of Physics
Friedrich-Alexander-Universität
Staudtstr. 2, 91058 Erlangen, Germany

Light fields carrying optical vortices have many potential applications, for example optical tweezers[7] and classical or quantum communications.[8,9] Brillouin laser with optical vortices has attracted interest,[10,11] since Brillouin scattering provides a narrow linewidth and a nonlinear response that is typically stronger than Kerr and Raman interactions in most transparent media. However, a major challenge in current SBS-related vortex emission schemes is maintaining the vorticity as the light circulates in the cavity; the mode controllers that are typically used require constant adjustment and introduce optical loss. The recent emergence of chiral (PCF)[12]—a unique platform for studying the behavior of light in chiral structures that are infinitely extended in the direction of the twist—has enabled investigation of SBS process in the presence of chirality.[13]

Here we report a vortex Brillouin fiber laser in which chiral PCF is used to robustly preserve circularly polarized vortex modes over long distances, permitting topology-selective Brillouin gain.[14] In particular, angular momentum conservation dictates that the topological charge and spin of the backward Brillouin signal are opposite in sign to those of the pump. Making use of this fact, we experimentally demonstrate stable Brillouin lasing in different-order circularly polarized vortex modes, supported by acoustic modes guided in the chiral PCF core. This differs from previous Brillouin lasers which do not lase on a vortex mode: rather the output light is converted to a desired vortex mode outside the laser.[10,11] Linewidth-narrowing in the laser cavity allows the frequency shift of each individual Brillouin gain peak to be measured with resolution of 10 kHz and accuracy of 520 kHz, corresponding to the laser linewidth and cavity free spectral range, respectively. The results are consistent with theoretical predictions. Vortex carrying Brillouin lasers have potential applications in narrow-linewidth sources for quantum information processing, twisted photon–phonon studies [15–17] and optical tweezers.

2. Results

2.1. Chiral Multicore Photonic Crystal Fiber

Two types of chiral multicore PCF were used in the measurements: C_3 PCF has threefold rotational symmetry with a twist
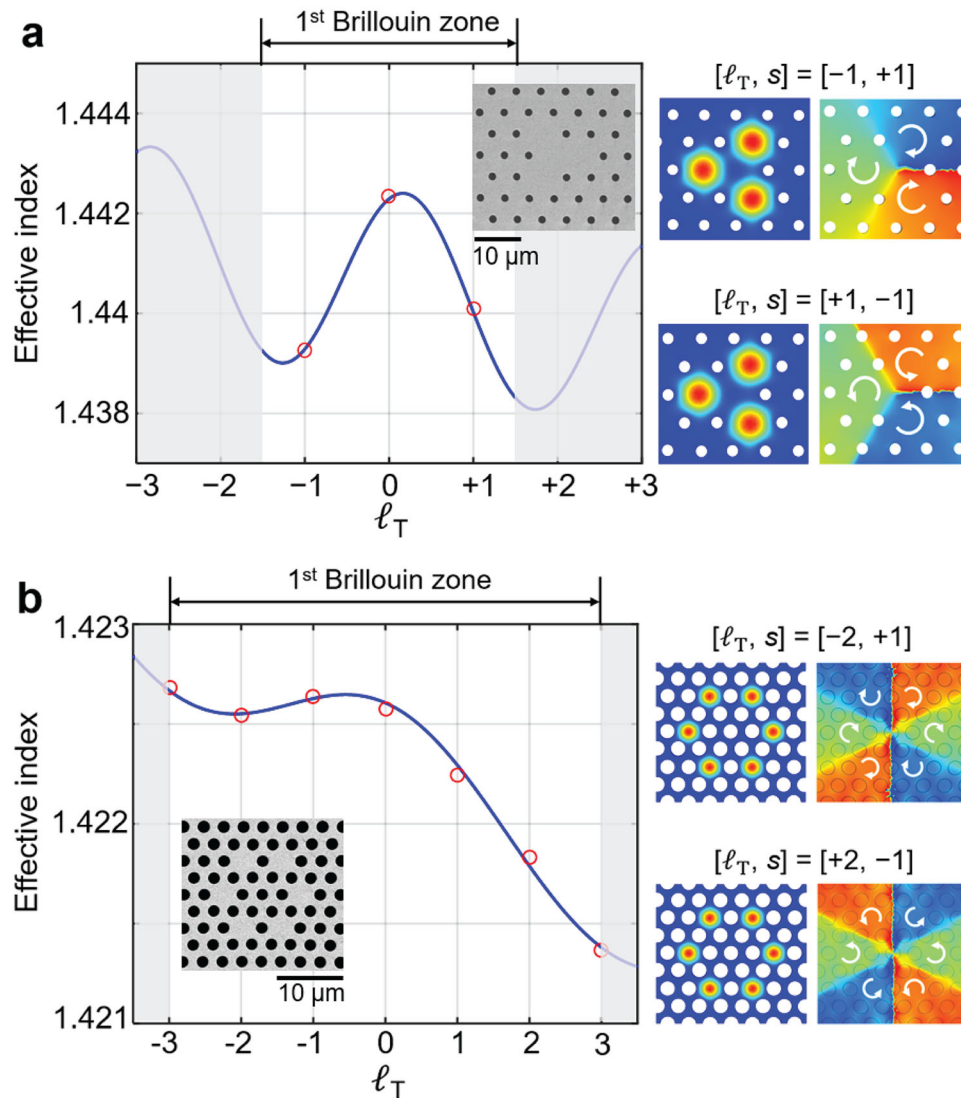
Figure 1. a) Calculated effective refractive index versus topological charge ℓ_T in C_3 PCF (left) and mode, phase and polarization states distributions (right) of $[+1, -1]$ and $[-1, +1]$ modes. The inset shows a scanning electron micrograph (SEM) of C_3 PCF. b) Same as (a), for PCF C_6.

Table 1. Fiber parameters..

	Satellite core diameter	Air-hole diameter	Inter-hole distance	Twist pitch
C_3 PCF	8.56 µm	1.6 µm	5.15 µm	5 mm
C_6 PCF	4 µm	2 µm	2.98 µm	7.2 mm

pitch of 5 mm [18] (inset in **Figure 1**a) and C_6 PCF has sixfold rotational symmetry with a twist pitch of 7.2 mm (inset in Figure 1b). The parameters of the two PCFs are shown in **Table 1**. Both chiral PCFs were formed by replacing specific preform capillaries with solid glass rods and drawing the fibers from a spinning preform. Chiral PCFs with N-fold rotationally symmetric (symmetry class C_N) support circularly polarized helical Bloch modes (HBMs) with mth order azimuthal harmonics that carry optical

vortices with azimuthal order $\ell_A^{(m)} = \ell_A^{(0)} + Nm$ ($\ell_A^{(0)}$ is the principal order). The $\ell_A^{(m)}$ is obtained in cylindrical coordinates and for pure circularly polarized fields can be related to the topological charge $\ell_T^{(m)}$ in Cartesian coordinates via $\ell_A^{(m)} = \ell_T^{(m)} + s$ (spin $s = +1$ for left-circular polarization) simply by rotating the reference frame. The shorthand $[\ell_T, s]$ will be used to denote each circularly polarized vortex-carrying HBM, where ℓ_T is defined to be $\ell_T^{(0)}$. Figure 1a,b shows the modal refractive indices (blue curves) in both C_3 and C_6 PCFs against topological charge ℓ_T, estimated from the analytical model.[19] The red circles are numerically calculated modal indices of each ℓ_T. Both $[\ell_T, +1]$ and $[\ell_T, -1]$ collapse on to one curve, as the modes with opposite spin are only very weakly birefringent. The calculated mode, phase and polarization states distributions of $[+1, -1]$, $[-1, +1]$, $[+2, -1]$, and $[-2, +1]$ modes are shown in Figure 1. The index difference is $\approx 8 \times 10^{-4}$ between $[+1, \pm1]$ and $[-1, \pm1]$ modes and $\approx 7 \times 10^{-4}$ between $[+2, \pm1]$ and $[-2, \pm1]$ modes. The measured loss of both
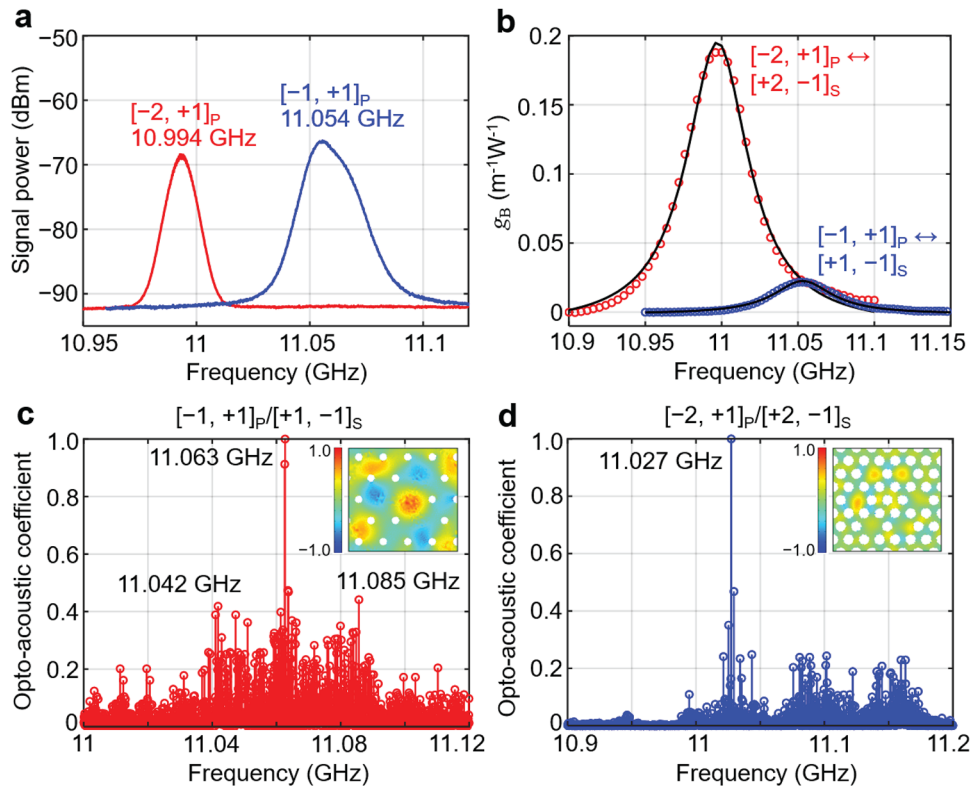
Figure 2. a) Spontaneous Brillouin spectra generated by 1550 nm pumping C_3 PCF with a 1 W $[-1, +1]_P$ mode (blue) and C_6 PCF with a 1 W $[-2, +1]_P$ mode (red). b) Measured Brillouin gain spectra for pumping the $[-1, +1]_P$ mode in C_3 PCF (blue) and the $[-2, +1]_P$ mode in C_6 PCF (red). The black lines are Lorentzian fits. c) Numerically calculated opto-acoustic coupling coefficients for each acoustic mode that satisfies phase-matching (see text), normalized to the highest value of κ. d) Same as (c), for C_6 PCF. The insets in (c) and (d) show the axial displacement (normalized to the square-root of the power) for the peaks at 11.063 and 11.027 GHz.

$[\pm 1, \pm 1]$ and $[\pm 2, \pm 1]$ modes are 0.017 and 0.04 dB m^{-1}, respectively.

2.2. Experimental Results

Details of the Brillouin measurement setup are available in the Experimental Section. **Figure 2**a shows the spontaneous Brillouin spectra measured after injecting a 1 W $[-1, +1]_P$ mode into a 200 m length of C_3 PCF and a 1 W $[-2, +1]_P$ mode into a 200 m length of C_6 PCF (subscript P denotes the pump mode). The Brillouin peak frequencies are 11.054 GHz for the $[-1, +1]_P$ mode and 10.994 GHz for the $[-2, +1]_P$ mode. The spontaneous Brillouin spectrum for $[-1, +1]_P$ pumping is slightly asymmetric, deviating from a perfect Lorentzian, which suggests that more than one acoustic mode is excited. Although it is impossible to resolve these closely spaced peaks by normal heterodyning techniques, they could be precisely measured when the linewidths of Stokes signals are narrowed during light circulation in the laser ring cavity (the details will be discussed later in this paper). Figure 2b shows the Brillouin gain spectra measured in 200 m lengths of PCF C_3 (blue) and PCF C_6 (red) using a specially designed pump-seed setup (see Experimental Section). As dictated by angular momentum conservation [14], the Brillouin gain is only significant when pump and seed have opposite spin and topological charge, reaching peak values of 0.022 W^{-1} m^{-1} for $[-1, +1]_P/[+1, -1]_S$

pump/seed and 0.19 W^{-1} m^{-1} for $[-2, +1]_P/[+2, -1]_S$, where subscript S denotes Stokes wave.

To confirm the experimental results, we used COMSOL software to calculate the opto-acoustic coupling coefficient:[20]

$$\kappa \propto \iint dx\,dy\, E_P E_S^* p_{ijkl} \epsilon_{kl} \qquad (1)$$

where E_P and E_S are the scalar electric field distributions of circularly polarized vortex-carrying pump and Stokes modes, p_{ijkl} is the elasto-optic tensor and ϵ_{kl} is the strain tensor associated with the acoustic mode. The material parameters, such as Young's modulus, Poisson's ratio and coefficient of thermal expansion, are set to the default values for fused silica in the COMSOL materials library. The acoustic wavevector is first set to $\Delta\beta = 2\pi(n_P + |n_S|)/\lambda_P$, and the frequencies of the acoustic modes (typically ≈ 500) that share this wavevector are calculated. Equation (1) is then evaluated for each of these modes, and the results normalized to the mode with the highest value of κ. Figure 2c shows the results for $[-1, +1]_P/[+1, -1]_S$ modes in the C_3 PCF, revealing that, although a large number of acoustic modes satisfy phase-matching within the frequency range from 11 to 11.12 GHz, only the modes at 11.063 GHz (corresponding to the experimental peak at 11.054 GHz) have significant overlap with the optical modes and thus are dominant. The inset shows power-normalized axial displacements of the acoustic mode at
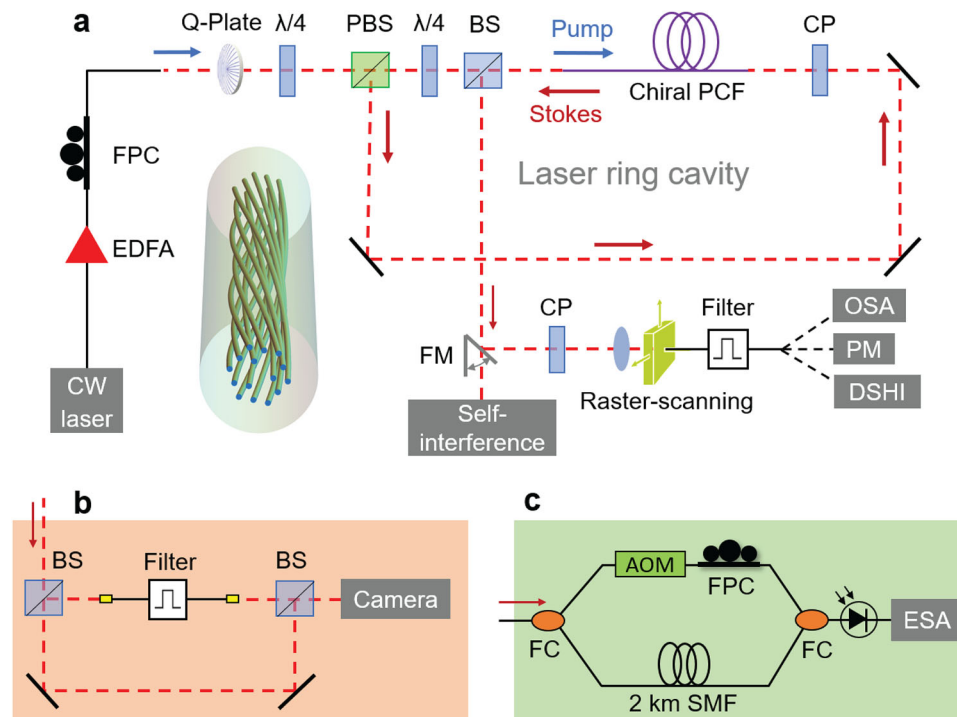
Figure 3. a) Experimental setup of vortex Brillouin laser. FPC: polarization controller, CP: circular polarizer, BS: beam splitter, PBS: polarizing beam splitter, $\lambda/4$: $\lambda/4$ plate, FM: flip mirror, OSA: optical spectrum analyzer, PM: power meter, DSHI: delayed self-heterodyne interference. Inset: 3D sketch of the chiral PCF. b) Experimental setup of spatial self-interference for Stokes topological charge measurement. c) Experimental setup of delayed self-heterodyne interference for laser linewidth measurement. AOM: acousto-optical modulator, FC: fiber coupler, SMF: single mode fiber.

11.063 GHz. However, it is possible that the calculated parasitic acoustic modes at 11.042 and 11.085 GHz are weakly excited in the experiment, causing the Brillouin spectrum to deviate from a perfect Lorentzian. Figure 2d shows the same calculations as Figure 2c, but for $[-2, +1]_P/[+2, -1]_S$ modes in C_6 PCF in the frequency range from 10.9 to 11.2 GHz. Although three peaks are obtained from the simulations, only the main peak at 11.027 GHz was experimentally observed (corresponding to the peak at 10.994 GHz). We attribute this to much weaker opto-acoustic coefficients, resulting in the other two peaks being below the noise floor.

Using 200 m lengths of C_3 and C_6 PCF we constructed two Brillouin fiber lasers generating different-order circularly polarized-vortex modes. The experimental setup is shown in **Figure 3**a. The continuous wave (CW) pump light passes sequentially through an erbium-doped fiber amplifier (EDFA), a polarization controller (FPC), a Q-plate, a $\lambda/4$ plate, a polarizing beam-splitter (PBS) and a second $\lambda/4$ plate, so as to launch a circularly polarized vortex mode into the laser. Since the Stokes signal is orthogonally polarized relative to the pump, it is reflected by the PBS and thus circulates inside the cavity. A circular polarizer (a combination of a $\lambda/4$ plate and a polarizer) blocks the transmitted pump light, while letting the backward Stokes signal propagate freely. A beam splitter (BS) was used to couple 10% of the laser signal out of the cavity and another circular polarizer enabled measurement of the Stokes polarization state. In order to precisely measure the mode profile at the laser output, we designed a near-field scanning Brillouin analyzer (NBA) that includes a fiber raster-scanning stage, a narrow-band (6 GHz)

filter and equipment for signal analysis (optical spectrum analyzer (OSA), power meter, delayed self-heterodyne interference system). The collected laser light, which contains small amounts of pump light (caused by Fresnel reflections or Rayleigh scattering), is collected pixel by pixel using a fiber raster scanning stage. The signal is then filtered to remove the pump frequency and then analyzed. An additional flip mirror was used to steer the laser beam into a self-interference setup (Figure 3b) for topological charge measurement. In the setup, the Stokes signal was split in two, one half being spatially filtered in a single-mode fiber to produce a divergent near-Gaussian beam which was then superimposed on the other half, resulting in spiral patterns of fringes related to the topological charge. These patterns were imaged using an infrared camera after filtering out any stray pump light with a narrow-band filter.

The laser output power is plotted against $[\pm 1, \pm 1]_P$ power in **Figure 4**a and $[\pm 2, \pm 1]_P$ power in Figure 4b. The threshold power, defined as the point at which the Stokes power equals 1% of the pump power, is 800 mW for $[\pm 1, \pm 1]_P$ and 700 mW $[\pm 2, \pm 1]_P$, with slope efficiencies of $\approx 2.9\%$ and $\approx 4.1\%$. Lasing commences when the Brillouin gain exceeds the laser cavity round-trip loss of 9.4 dB for PCF C_3 and 12 dB for PCF C_6. The cavity length was adjusted so that a single cavity mode coincided with the maximum Brillouin gain. The cavity included 200 m of PCF and 2.2 m of free space, resulting in a free spectral range of ≈ 520 kHz, which given the 45 MHz FWHM Brillouin gain linewidth means that 86 cavity longitudinal laser modes can participate in lasing. However, in a situation with strong mode competition,[21] only one mode survives and oscillates in the laser cavity. Note that both
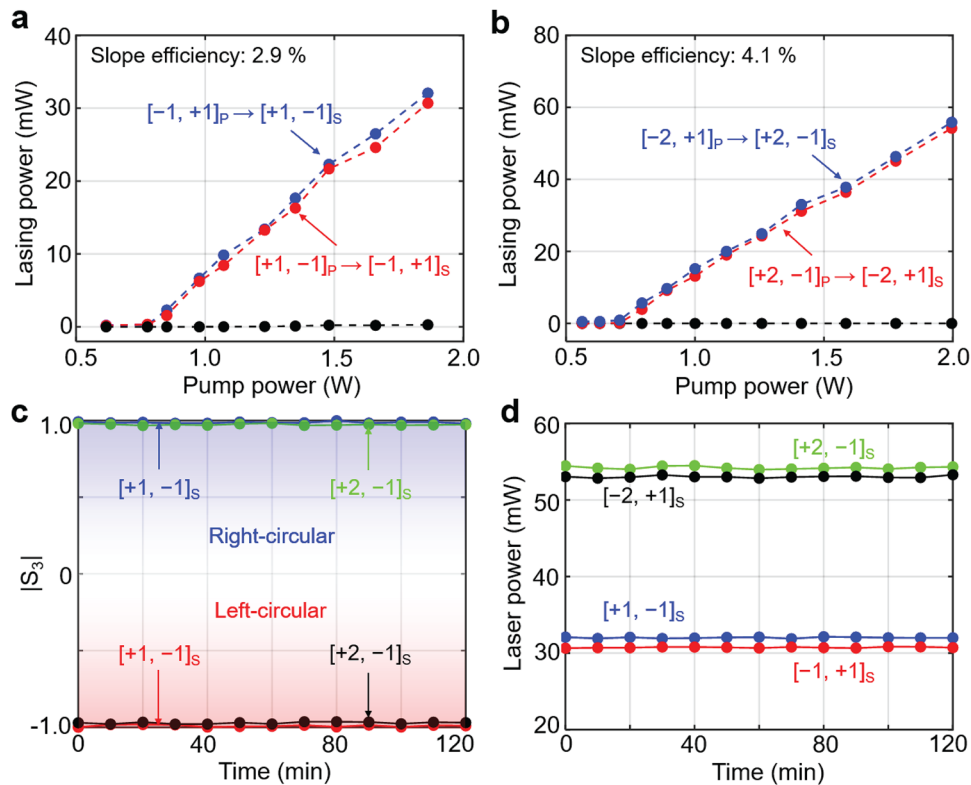
Figure 4. a) Output power of $[+1, -1]_S$ and $[-1, +1]_S$ Brillouin lasers in C_3 PCF, as a function of $[-1, +1]_P$ and $[+1, -1]_P$ power. b) Output power of $[+2, -1]_S$ and $[-2, +1]_S$ Brillouin lasers in C_6 PCF, as a function of $[-2, +1]_P$ and $[+2, -1]_P$ power. c) The measured Stokes parameter $|S_3|$ of $[+1, -1]_S$ (blue), $[-1, +1]_S$ (red), $[+2, -1]_S$ (green) and $[-2, +1]_S$ (black) vortex laser output over 2 h. d) Laser output power monitored over 2 h.

the threshold power and slope efficiency for $[+\ell_T, s]_P$ and $[-\ell_T, s]_P$ pumping are almost the same. This is because an identical acoustic mode is excited in each case. Nevertheless, some tiny differences are still observed in the two cases and we attribute this to slight circular dichroism in propagation loss. According to helical Bloch theory,[19] any deviations from integer values of topological charge are caused by the polarization state not being exactly circular. For the Brillouin lasers reported here, the measured Stokes parameter (S_3) had a modulus greater than 0.96 (Figure 4c), indicating very good preservation of circular polarization state, and yielding pure vortex modes with integer-valued topological charge at the laser output. Thanks to robust preservation of circular polarization state and topological charge in chiral PCF, the power stability of the vortex Brillouin lasers was very good (fluctuations of <1% over 2 h, see Figure 4d), and higher than those of all-fiber Brillouin lasers where the output is externally converted to different OAM modes.[10] Since the Brillouin scattering effect is quite sensitive to environmental changes (e.g., mechanical vibration, temperature, and air pressure changes), the vortex lasers displayed longitudinal mode instability (within the 1 MHz range). However, this can easily be suppressed by proper environmental isolation.

The spectrum measured by the high-resolution OSA just before the filter confirmed the presence of a $[+1, -1]_S$ laser signal with frequency 11.054 GHz below the pump frequency (**Figure 5**a). The upper panels of Figure 5b show the near-field profiles of $[-1, +1]_P$ and $[-2, +1]_P$ pump light measured by the camera,

together with the spiral fringe patterns measured by interference with a divergent Gaussian beam. The lower panel of Figure 5b shows the near-field profiles of the corresponding laser signals measured by the NBA system, along with their spiral fringe patterns. Again, it is seen that pump and laser signals have opposite topological charge and spin. Since grating-based OSAs and Fabry–Perot interferometers typically have insufficient spectral resolution (a few GHz and tens of MHz respectively),[22] we implemented a "sub-coherence" delayed self-heterodyne interference (DSHI),[23] which is capable to measure sub-kHz linewidths. Figure 3c shows the measurement setup. The Brillouin laser output is launched into an SMF and split into two paths at a 3 dB fiber coupler. One path is frequency-shifted by 200 MHz using an acousto-optic modulator (AOM), and the other path is transmitted through a 2 km length of SMF, so that it becomes sub-correlated from the frequency-shifted light. Figure 5c,d shows the measured spectra of $[+1, -1]$ and $[+2, -1]$ vortex Brillouin lasers. The sharp side-peaks close to the center are artefacts from mechanical vibrations in the pump laser. Linewidths of 10 kHz for $[+1, -1]$ Brillouin laser and 8 kHz for $[+2, -1]$ Brillouin laser were obtained by fitting the measured laser spectra to the sub-coherence lineshape function. A comparison between lasing and spontaneous Stokes spectra (generated without optical cavity feedback) shows a line-narrowing factor of $\approx 4 \times 10^3$ for the $[+1, -1]_S$ laser and $\approx 5 \times 10^3$ for the $[+2, -1]_S$ laser (Figure 5c,d).

As discussed in Figure 2a, the spontaneous Brillouin spectra for $[\pm 1, \pm 1]_P$ pump modes in C_3 PCF are slightly asymmet-
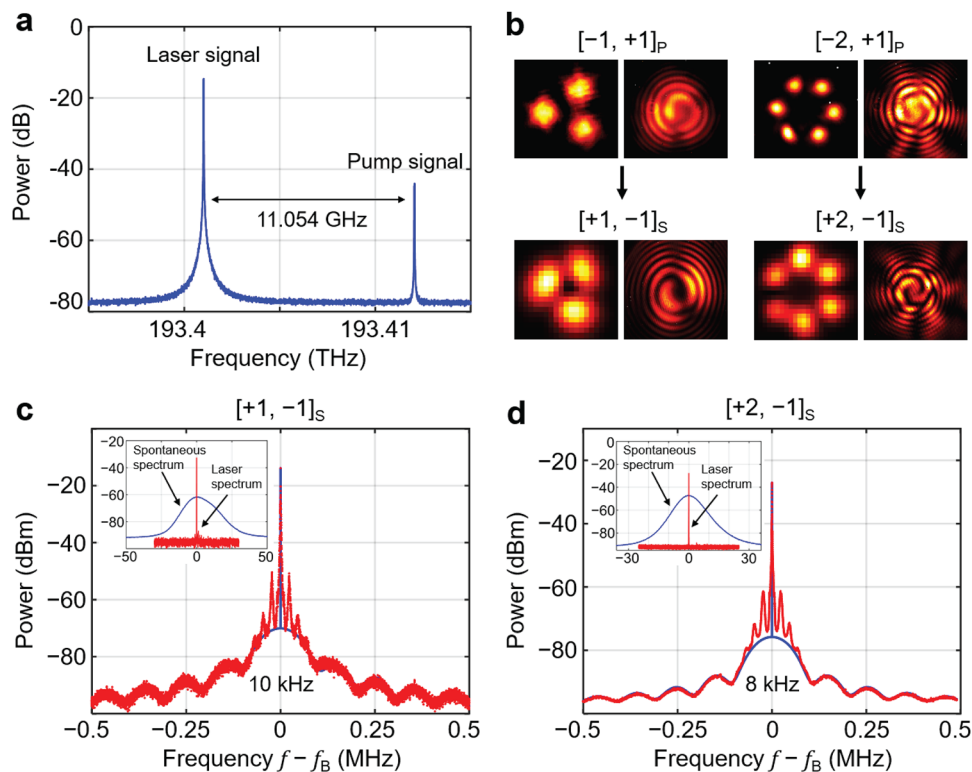
Figure 5. a) Power spectrum of $[+1, -1]_S$ laser output before the narrow-band filter, measured by the OSA. b) Measured mode profiles and interferometric spiral fringe patterns of $[-1, +1]_P$ (or $[-2, +1]_P$) pump and $[+1, -1]_S$ (or $[+2, -1]_S$) vortex Brillouin laser signals; c) The laser spectrum (red) for the $[+1, -1]_S$ mode in C₃ PCF, measured by sub-coherence delayed self-heterodyning and compared with a theoretical fit (blue). The inset compares the spontaneous Stokes spectrum from C₃ PCF with the line-narrowed intracavity laser spectrum measured by delayed self-heterodyne system (the axis labels are same as those of main figure, f_B is the Brillouin frequency). d) Same as (c), for the $[+2, -1]_S$ lasing mode in C₆ PCF.
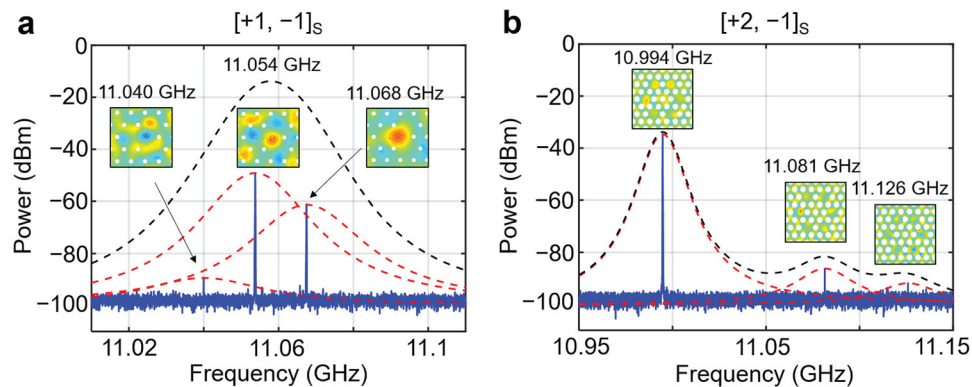

Figure 6. a) The spectrum of the $[+1, -1]_S$ lasing mode in C₃ PCF, measured by heterodyning the laser signal with a local oscillator at the pump frequency. The red dashed curves show the calculated Lorentzian functions for three Brillouin peaks and the black dashed curve their superposition. Insets, normalized axial displacements of three acoustic modes. b) Same as (a), but for lasing in the $[+2, -1]_S$ mode in C₆ PCF.

ric, deviating from perfect Lorentzian lineshapes. This can be attributed to weak excitation of other acoustic modes, causing Brillouin shifts only ≈20 MHz away from the main peak. Although these closely spaced peaks are difficult to be resolved experimentally by spontaneous scattering or pump–probe techniques, precise measurements can be made using the line-narrowing associated with Brillouin lasing. **Figure 6**a shows the spectrum obtained by normal heterodyning between the laser signal and a lo-

cal oscillator at the pump frequency. Three Brillouin lasing peaks are seen, at 11.04, 11.054, and 11.068 GHz (blue curve), the one at 11.054 GHz being the strongest. The experimental results are in excellent agreement with the simulations in Figure 2c. The insets show the normalized axial displacement of the three associated acoustic modes. Linewidth-narrowing to ≈10 kHz permits the center-band frequencies of the three peaks to be easily resolved. For comparison, the red dashed curves show the indi-
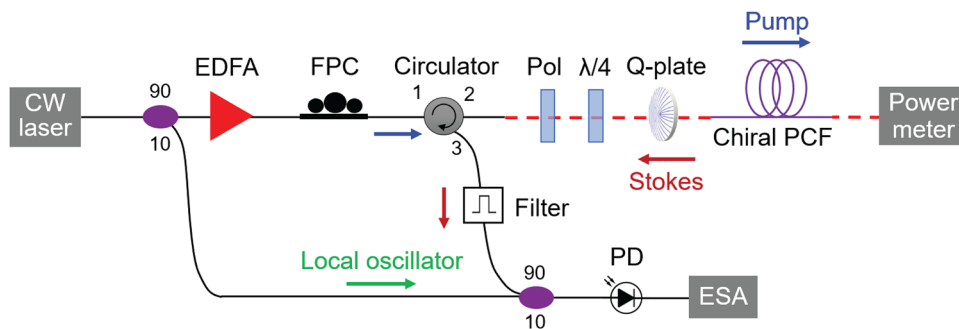
Figure 7. Heterodyne setup for the measurement of spontaneous Brillouin spectra. Pol: polarizer. .

vidual Lorentzian-shaped spectra for each of the three peaks in the absence of line-narrowing, and the black dashed curve their superposition, showing an asymmetry similar to that seen in the spontaneous Brillouin spectrum in Figure 2a (blue curve). This technique allows much more accurate measurements (within the cavity free spectral range of ≈520 kHz) of the Brillouin frequency shifts than is possible from the spontaneous Brillouin spectrum, with a precision can be further improved by extending the fiber length.

Figure 6b shows the results for $[-2, +1]_P$ and $[+2, -1]_S$ modes in C_6 PCF. Three peaks at 10.994, 11.081, and 11.126 GHz are easily resolved, showing good agreement with the simulations in Figure 2d. However, in the spontaneous Brillouin measurement in Figure 2a (red curve), a symmetric Lorentzian-shaped spectrum without side-peak was only observed. We attribute this to different interaction strengths in the spontaneous and lasing cases, the two additional Brillouin peaks being too weak to be spontaneously excited. We note in addition that line-narrowing in a Brillouin laser cavity can be potentially used in photoacoustic spectroscopy [24] and fiber sensing.[4]

3. Discussion and Conclusion

Optoacoustic interactions between optical vortices and guided acoustic modes in twisted PCF give rise to chiral stimulated Brillouin scattering in which power is transferred between pump and Stokes modes with opposite topological charge and spin. This makes possible, for the first time to our knowledge, stable laser oscillation of optical vortices in a Brillouin laser cavity (we note that although annular core fibers [25] may potentially be used to construct vortex Brillouin lasers, they have not been shown to maintain circular polarization state). We note that Brillouin scattering between vortex modes with different topological charge may also occur if the acoustic mode itself carries non-zero topological charge.[15]

In contrast to previous lasers based on SBS, the vortex Brillouin lasers reported in this paper intrinsically maintain the vorticity of light in the whole laser cavity without need for mode control techniques. Laser line-narrowing permits the closely spaced Brillouin peaks associated with different acoustic modes to be precisely resolved, in excellent agreement with theoretical predictions.

We emphasize that, in addition to preserving circular polarization state, the helical Bloch modes supported by chiral PCF are unique in displaying twist-rate-dependent topological bire-

fringence, i.e., modes with equal and opposite topological charge have different propagation constants. This makes it possible to construct a Brillouin fiber laser that directly emits stable vortex modes, unlike previous Brillouin lasers based on conventional non-chiral few-mode fibers, which do not provide any spin or topological birefringence, and can only produce a vortex output by means of external components, limiting the bandwidth of operation. In contrast, vorticity and spin are intrinsically maintained within the chiral laser cavity over an ultra-broad bandwidth from the visible to the infrared.

Chiral PCF also supports torsional-radial acoustic vortex modes that can cause SBS between optical modes with different topological charge, opening up further opportunities. Use of chiral PCF made from non-silica glasses such as the chalcogenides As_2Se_3 or As_2S_3 [26] would result in lasers with higher slope efficiencies.

Vortex Brillouin lasers based on chiral PCF are of potential interest in many areas, for example, combined with multi-frequency Brillouin scattering,[27] they can potentially be used in mode-division-multiplexing.[8] They can be used in high-dimensional quantum entanglement,[28,29] which shows stronger nonclassical correlations than two-photon polarization entanglement.[30] Line-narrowing in chiral vortex Brillouin lasers allows high resolution spectroscopy of photoacoustic interactions in twisted PCF. Vortex Brillouin lasers are also of interest in optical tweezers [31] and in atom/nano-particle cooling,[32] which requires narrow linewidths (sub-10 kHz, directly available from the laser) to drive the transitions. Finally, SBS in chiral PCF opens up new perspectives for increasing the storage capacity of optical memories, by using each vortex mode as a different channel.[27,33]

4. Experimental Section

Heterodyne Measurement Setup: The Heterodyne measurement setup is shown in **Figure 7**. The Light from a narrow linewidth (<1 kHz) 1550 nm CW laser was split into pump and local oscillator (LO) signals at a fiber coupler. The pump signal was then amplified in an EDFA and launched into the chiral PCF via an optical circulator. The circular polarization state was adjusted using a FPC placed before the circulator. The vortex generating module (polarizer, $\lambda/4$ plate and Q-plate) was optionally used to generate a circularly polarized vortex-carrying pump signal. The noise-seeded Stokes signal from the PCF was delivered by the circulator and interferes with the LO signal using a second 90:10 fiber coupler. Narrow-band (6 GHz) notch filters placed in the path of the Stokes signal were used to filter out Fresnel reflections and Rayleigh scattering. The resulting beat-note was
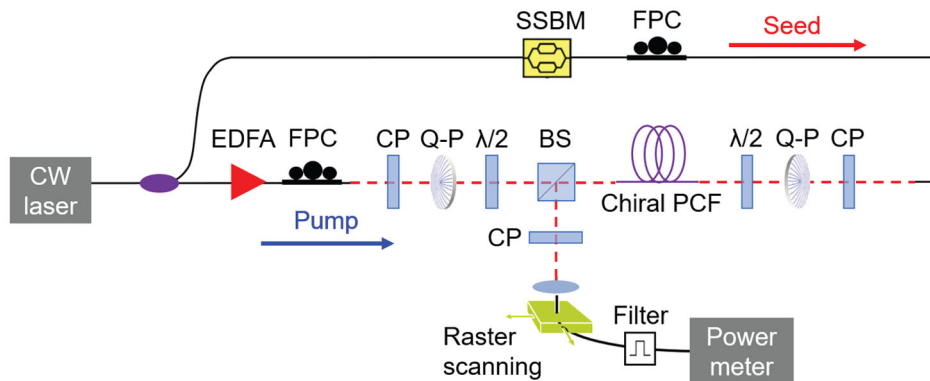
Figure 8. Pump-seed experimental setup for gain coefficient measurement. Q-P: Q-plate. $\lambda/2$: $\lambda/2$ plate.

detected in the radio-frequency domain using a fast photodiode (PD) and the averaged Brillouin spectra were recorded with an electrical spectrum analyzer.

Pump-Seed Setup: The pump-seed setup is shown in **Figure 8**. Both pump and seed were derived from a narrow linewidth 1550 nm CW laser, the seed light being frequency tuned using a single side-band modulator (SSBM). The pump signal was boosted by an EDFA and the polarization states of both pump and seed were controlled using FPCs. Vortex generating modules (circular polarizer, Q-plate and $\lambda/2$ plate) were optionally used to generate circularly polarized vortex-carrying pump signals. After propagating backward through the chiral PCF and interacting with pump signal, the seed signal was reflected by a beam splitter (BS), filtered by a circular polarizer (polarizer and $\lambda/4$ plate) and finally delivered to NBA system for gain coefficient measurement.

Conflict of Interest

The authors declare no conflict of interest.

Data Availability Statement

The data that support the findings of this study are available from the corresponding author upon reasonable request.

[1] R. Y. Chiao, C. H. Townes, B. P. Stoicheff, *Phys. Rev. Lett.* **1964**, *12*, 592.

[2] A. Kobyakov, M. Sauer, D. Chowdhury, *Adv. Opt. Photonics* **2010**, *2*, 1.

[3] B. J. Eggleton, C. G. Poulton, P. T. Rakich, M. J. Steel, G. Bahl, *Nat. Photonics* **2019**, *13*, 664.

[4] J. B. Murray, A. Cerjan, B. Redding, *Optica* **2022**, *9*, 80.

[5] S. P. Smith, F. Zarinetchi, S. Ezekiel, *Opt. Lett.* **1991**, *16*, 393.

[6] J. Li, M.-G. Suh, K. Vahala, *Optica* **2017**, *4*, 346.

[7] M. Chen, M. Mazilu, Y. Arita, E. M. Wright, K. Dholakia, *Opt. Lett.* **2013**, *38*, 4919.

[8] N. Bozinovic, Y. Yue, Y. Ren, M. Tur, P. Kristensen, H. Huang, A. E. Willner, S. Ramachandran, *Science* **2013**, *340*, 1545.

[9] G. Vallone, V. D'Ambrosio, A. Sponselli, S. Slussarenko, L. Marrucci, F. Sciarrino, P. Villoresi, *Phys. Rev. Lett.* **2014**, *113*, 060503.

[10] J. Wang, J. Zhang, A. Wang, X. Jiang, J. Yao, Q. Zhan, *Opt. Express* **2021**, *29*, 18408.

[11] J. Xu, L. Zhang, X. Liu, L. Zhang, J. Lu, L. Wang, X. Zeng, *Opt. Lett.* **2021**, *46*, 468.

[12] P. St J Russell, R. Beravat, G. K. L. Wong, *Philos. Trans. R. Soc., A* **2017**, *375*, 20150440.

[13] X. Zeng, W. He, M. H. Frosz, A. Geilen, P. Roth, G. K. L. Wong, P. St J Russell, B. Stiller, *Photonics Res.* **2022**, *10*, 711.

[14] X. Zeng, P. St J Russell, C. Wolff, M. H. Frosz, G. K. L. Wong, B. Stiller, (preprint) arXiv:2203.03680, unpublished **2022**.

[15] H. H. Diamandi, G. Bashan, Y. London, K. Sharma, K. Shemer, A. Zadok, *Laser Photonics Rev.* **2021**, *16*, 2100337.

[16] Z. Zhu, W. Gao, C. Mu, H. Li, *Optica* **2016**, *3*, 212.

[17] S. Gspan, A. Meyer, S. Bernet, M. Ritsch-Marte, *J. Acoust. Soc. Am.* **2004**, *115*, 1142.

[18] P. Roth, M. H. Frosz, L. Weise, P. St J Russell, G. K. L. Wong, *Opt. Lett.* **2021**, *46*, 174.

[19] Y. Chen, P. St. J. Russell, *J. Opt. Soc. Am. B* **2021**, *38*, 1173.

[20] V. Laude, A. Khelif, S. Benchbane, M. Wilm, T. Sylvestre, B. Kibler, A. Mussot, J. M. Dudley, H. Maillotte, *Phys. Rev. B* **2005**, *71*, 045107.

[21] R. L. Fork, M. A. Pollack, *Phys. Rev.* **1965**, *139*, A1408.

[22] B. Daino, P. Spano, M. Tamburrini, S. Piazzolla, *IEEE J. Quantum Electron.* **1983**, *19*, 266.

[23] L. Richter, H. Mandelberg, M. Kruger, P. McGrath, *IEEE J. Quantum Electron.* **1986**, *22*, 2070.

[24] Q. Wang, Z. Wang, J. Chang, W. Ren, *Opt. Lett.* **2017**, *42*, 2114.

[25] P. Gregg, P. Kristensen, S. Ramachandran, *Optica* **2015**, *2*, 267.

[26] C. Fortier, J. Fatome, S. Pitois, F. Smektala, G. Millot, J. Troles, F. Desevedavy, P. Houizot, L. Brilland, N. Traynor, in Eur. Conf. Opt. Commun. paper Th.2.B.3, **2008**.

[27] B. Stiller, M. Merklein, K. Vu, P. Ma, S. J. Madden, C. G. Poulton, B. J. Eggleton, *APL Photonics* **2019**, *4*, 040802.

[28] W. Löffler, T. G. Euser, E. R. Eliel, M. Scharrer, P. St J Russell, J. P. Woerdman, *Phys. Rev. Lett.* **2011**, *106*, 240505.

[29] R. Fickler, R. Lapkiewicz, W. N. Plick, M. Krenn, C. Schaeff, S. Ramelow, A. Zeilinger, *Science* **2012**, *338*, 640.

[30] A. Poppe, A. Fedrizzi, R. Ursin, H. R. Böhm, T. Lorünser, O. Maurhardt, M. Peev, M. Suda, C. Kurtsiefer, H. Weinfurter, T. Jennewein, A. Zeilinger, *Opt. Express* **2004**, *12*, 3865.

[31] Z. Hu, L. K. Kang, *J. R. Soc., Interface* **2008**, *5*, 671.

[32] J. W. R. Tabosa, D. V. Petrov, *Phys. Rev. Lett.* **1999**, *83*, 4967.

[33] B. Stiller, M. Merklein, C. Wolff, K. Vu, P. Ma, S. J. Madden, B. J. Eggleton, *Optica* **2020**, *7*, 492.